Springer

KSME

Journal of Mechanical Science and Technology 24 (2010) 429~440
www.springerlink.com/content/1738-494x
DOI 10.1007/s12206-009-1105-x

# Unsteady boundary layer for a pitching airfoil at low Reynolds numbers †

Dong-Ha Kim[1] and Jo-Won Chang[2,*]

[1]*Research Associate, Department of Aerospace and Mechanical Engineering, Korea Aerospace University*
[2]*Associate Professor, Department of Aeronautical Science and Flight Operation, Korea Aerospace University, Goyang-city, Gyeonggi-do, 412-791, Korea*

(Manuscript Received June 19, 2009; Revised August 8, 2009; Accepted August 31, 2009)

**Abstract**

An experimental study was conducted in order to investigate unsteady boundary layers for a pitching airfoil. An NACA0012 airfoil sinusoid-pitched at quarter chord was employed, and its mean angle-of-attack and oscillation amplitude were 0° and 6°, respectively. To explore the unsteady boundary layers, smoke-wire visualization and surface-mounted probe measurements were pursued for three different cases, varying with Reynolds numbers ($Re_c$=2.3×10$^4$, 3.3×10$^4$, and 4.8×10$^4$). A reduced frequency of 0.1 was identically set in all cases. Results show that in the presented Reynolds number range, the separation bubble dependent on both angle-of-attack and Reynolds number was observed, accompanied with unsteady laminar separation after reattachment. The unsteady laminar separation occurred at the saddle point, which was formed by the two vortices, the wall, and the external flow, and it was independent of reverse flow. This result indicates that the unsteady laminar separation occurs during the process of transition after the reattachment of separated boundary layer for an unsteady flow. The reverse flow observed over the trailing edge significantly interacted with the trailing edge vortex that rotates in the streamwise direction. This trailing edge vortex prevents the uppermost of the reverse flow from reaching to the unsteady laminar separation point during the upstroke, and this induces that the boundary layer breakdown does not occur in spite of the occurrence of laminar separation. The discrete vortices are formed by unsteady laminar separation, and its formation is ultimately affected by the Reynolds number. Consequently, it is obvious that the unsteady boundary layers are ultimately sensitive to Reynolds number in a low Reynolds number regime.

*Keywords*: Unsteady boundary layer; Pitching airfoil; Unsteady laminar separation; Reynolds number effects

## 1. Introduction

The unsteady flow that emerges from the operation of helicopter rotor blades, aircraft propellers, and turbine blades is largely divided into two types: post- and pre-stall. In the post-stall regime, the separation point moves towards the leading edge. Leading edge vortex, free shear layer, and inviscid-viscous interaction occur eventually, and these flow structures play an important role in dynamic stall [1, 2].

On the other hand, in the pre-stall regime, the time delay composed of both the circulation lag and boundary layer convection lag dominates an unsteady boundary layer [3]. The time delay directly influences the flow before boundary layer separation. From this point of view, the motion direction of the airfoil for a pitching airfoil is an important parameter since boundary layer velocity in the vicinity of the stagnation point is accelerated or exhibits an inflection point according to the airfoil motion [4].

For an unsteady boundary layer in a low Reynolds number range, the mechanism of unsteady laminar separation is very complicated and ambiguous. Reverse flow can occur without boundary layer breakdown, which means that even though the reverse flow occurs, the boundary layer may not be broken-down [5, 6]. Additionally, vanishing of the shear stress is no longer an indicator of unsteady laminar separation [7]. Koromilas and Telionis [8] experimentally investigated unsteady laminar separation in three models by varying the adverse pressure gradients for the Reynolds number around 10$^4$. They suggested that the unsteady laminar separation occurred at a saddle point consisting of the reverse flow upstream and the vortex downstream of an unsteady laminar separation. They proved the criterion of unsteady laminar separation ($du/dy = 0$ at $u = 0$, where $du/dy$ is a streamwise velocity gradient along the normal direction against the body surface) against laminar separation ($du/dy = 0$ at $y = 0$), indicating that zero shear stress does not always coincide with unsteady laminar separation.

In the pre-stall regime, Kim and Park [9] carried out smoke-

† This paper was recommended for publication in revised form by Editor Haecheon Choi

*Corresponding author. Tel.: +82 2 300 0082, Fax.: +82 2 3158 1849
E-mail address: jwchang@kau.ac.kr.

wire visualization for a pitching airfoil. They guessed the unsteady laminar separation by the discrete vortices at the specific angle-of-attack and discussed the reduced frequency effects on the unsteady boundary-layer events. Also, Park *et al*. [10] measured the near-wakes behind an oscillating airfoil using hot-wire in the same facility that Kim and Park [9] had used earlier and suggested various wake characteristics dependent on unsteady laminar separation and trailing edge vortex; however, they did not identify the unsteady laminar separation over the airfoil surface.

In general, it is well known that dynamic stall is critically affected by both reduced frequency and oscillation amplitude. With respect to the Reynolds number effects, Ohmi et al. [11] reported that they are not dominant factors in $Re_c=1.5\times10^3$~$1.0\times10^4$ and high incidence elliptic airfoils. However, since the boundary layer events are sensitive to Reynolds number in the low Reynolds number range, the prediction of boundary layer events is difficult. In this context, Oshima and Ramaprian [12], after investigating the flow for a pitching airfoil using PIV (particle image velocimetry), suggested that flow characteristics can be discerned in $Re_c=1.8\times10^4$~$5.4\times10^4$. They noted that at $Re_c=1.8\times10^4$, a shear layer vortex remained after dynamic stall. This led to a different flow structure compared to other Reynolds number cases. Chang [13] also discussed the influence of Reynolds numbers using an NACA4412 airfoil within low oscillating amplitude in $Re_c=5.3\times10^4$~$1.9\times10^5$. Recently, Laitone [14, 15] measured in detail the lift using a high accuracy balance on the stationary NACA0012 airfoil in the low Reynolds number range. They reported the unusual lift variation in the angles-of-attack of 3°~12°, and their results suggest that the boundary layer events in a low Reynolds number are still of interest. Therefore, more research and proof with respect to Reynolds number effects are necessary for low Reynolds number regime.

Substantially, when approaching the stall angle for a pitching airfoil, because the dependence on Reynolds number almost disappears, previous research that has focused on dynamic stall may have shown some limited results with respect to Reynolds number effects. Also, if one conducts an experiment to observe the Reynolds number effects, testing over the entire Reynolds number range is difficult. Furthermore, because the unsteady boundary layer is essentially influenced by various variables: for example, reduced frequency, mean angle-of-attack, oscillation amplitude, Reynolds number, adverse pressure gradient, body shape, free-stream turbulence, and surface irregularity, it is obvious that in spite of previous efforts, the unsteady laminar separation in a low Reynolds number range is still an open area. Therefore, we need more elaborate results in an unsteady boundary layer to apply to various flow fields.

The objectives in the present paper are to investigate an unsteady boundary layer and to evaluate Reynolds number effects for an unsteady boundary layer within stall angle-of-attack using a pitching NACA0012 airfoil in a low Reynolds number regime. The unsteady boundary layers were visualized by smoke-wire technique in order to obtain a physical understanding of the flow structure. A position over the airfoil surface was selected as the location of the smoke-wire. The oscillating amplitude was set to eliminate dynamic stall, and the three Reynolds number cases were employed after preliminary testing.

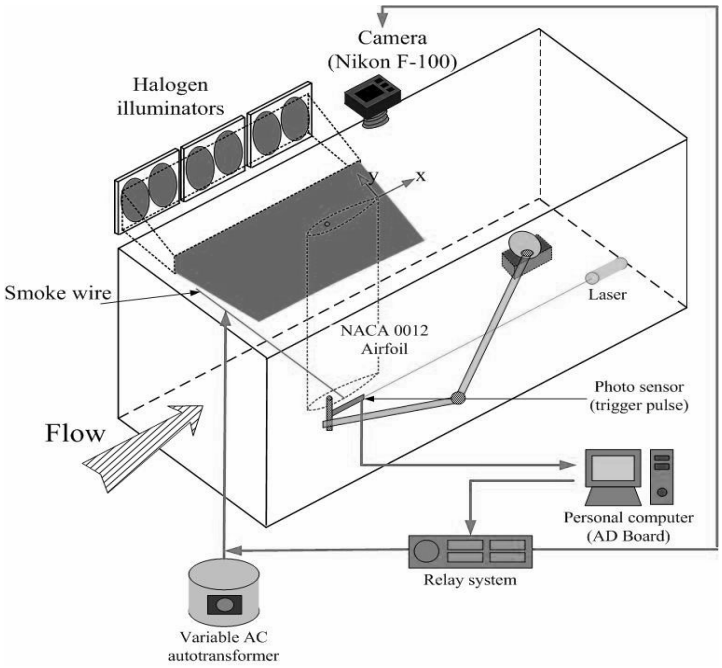


Fig. 1. Schematic of test section and airfoil oscillation system.

## 2. Experimental set-up and procedure

### *2.1 Wind tunnel and visualization system*

Fig. 1 illustrates the schematics of the test section and oscillating system. The experiments were conducted in a low speed wind tunnel, which is an open suction type. The size of test section was 0.5m (H)×0.5m (W)×1.4m (L) and had a contraction ratio of 7.2:1. The cross section of the model was an NACA0012 with a chord length of 0.18m, and it was set up in the test section vertically. The gap between the test-section side wall and the airfoil was less than 2.5mm in order to minimize a three-dimensional effect. The airfoil was pitched at the quarter chord using two connecting rods with a circular disk and an adjustable AC motor. The instantaneous angle-of-attack can be written as $\alpha(t) = 0^\circ + 6^\circ \sin \omega t$, the mean angle-of-attack was 0°, and the oscillation amplitude was 6°. Fig. 2 shows a comparison between the measured instantaneous angle-of-attack (experimental data) using an encoder and $\alpha(t) = 0^\circ + 6^\circ \sin \omega t$ (numerical data) at the corresponding frequency of the airfoil. Good agreement is observed between them. Tests were carried out at three free-stream velocities of 1.98, 2.83, and 4.03m/s, and the corresponding Reynolds numbers based on the chord length were $Re_c$=2.3×10$^4$, 3.3×10$^4$, and 4.8×10$^4$. A reduced frequency defined as $K = \omega C / 2U_\infty$ was fixed at 0.1 in all cases. The corresponding oscillating frequencies of the airfoil were 0.350, 0.500, and 0.717Hz in each case.

For the smoke-wire visualization, the locations of the light source and camera in the test-section are shown in Fig. 1. To visualize the flow in the neighbourhood of the airfoil, a Teikoku Alloy wire with a diameter of 0.14mm was horizontally installed at 0.33C ahead of the leading edge and at 0.8C in the spanwise direction. Additionally, a wire of 0.1mm diameter was vertically installed at 0.06C behind the leading edge and at a distance of about 1.0mm above the airfoil surface. Both wires described above were activated simultaneously for boundary layer visualization. Also, a wire with a diameter of 0.14mm was installed 3mm downstream from the trailing edge to order to visualize reverse flow. A sheet beam was generated using six halogen illuminators of 1kW each, and a Nikon F-100 camera was used with a shutter speed of 1/160~1/200 sec. The profile view pictures were obtained by a camera at the top side of the test section.

When implementing unsteady flow visualization, it is necessary to control the starting time of the camera to take pictures at the desired angle-of-attack. Also, since the duration of the smoke is very short (2-3sec.), the starting time for smoke release must be controlled in synchronization with the camera and the airfoil motion. Thus, a special synchronization system using two electronic relay systems was designed and quantitatively handled by a personal computer. Through the above synchronized control system, photographs can be taken at the optimum quantity of smoke. The photographs were intensively obtained in the range of interesting angle-of-attack at a fine interval, and its error was less than 0.2°. During the tests, the variation of free-stream velocity was less than 2.8%, and the temperature variation maxed out at 0.9℃.

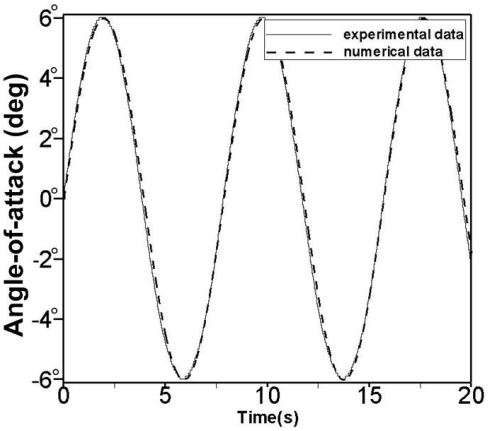


Fig. 2. Instantaneous angle-of-attack.

### *2.2 Surface-mounted probes*

A surface-mounted probe can measure the shear stress of an unsteady boundary layer with proper calibration. However, the calibration is very complicated and various sources of uncertainty exist because the surface-mounted probe measures the shear stress using the heat transfer between the probe and the flow. The amount of heat transfer is affected by a number of undesired variables such as airfoil material, strength of attachment, substrate material, and the reference flow properties [16]. In the present paper, the surface-mounted probe was not calibrated, and the obtained results were qualitatively analyzed.

Dantec's hot-film sensor (Glue-on type, 55R47) was employed as the surface-mounted probe on the CTA (constant temperature anemometry) system. The total size of the glue-on probe was 8.0mm×16.0mm, the sensor size was 0.1mm×0.9mm, and the thickness was less than 50 $\mu m$ (Fig. 3). It was connected to the gold-plated lead areas and was deposited on Kapton$^{TM}$ foil. Eighteen glue-on probes divided into three groups were used and were diagonally installed in order to avoid interference between the probes. Each probe

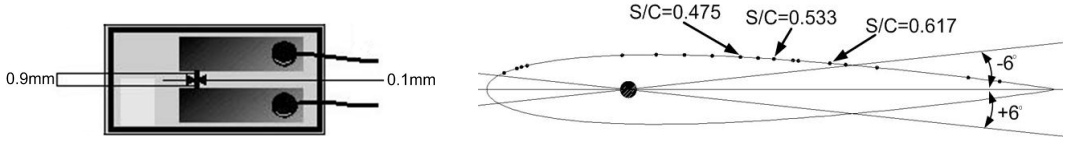


Fig. 3. Glue-on probe and its positions on the airfoil surface.

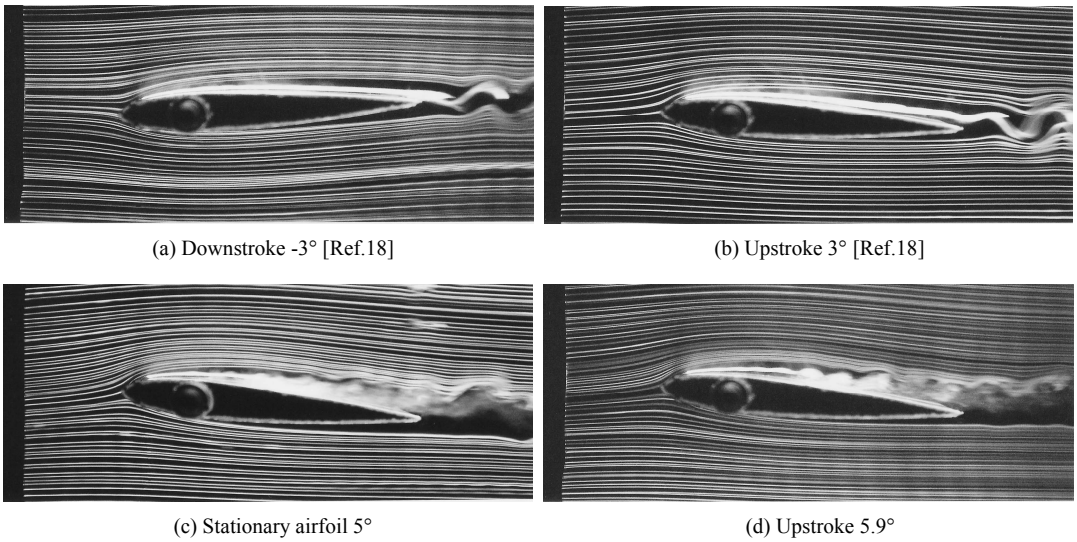

(a) Downstroke -3° [Ref.18] (b) Upstroke 3° [Ref.18]

(c) Stationary airfoil 5° (d) Upstroke 5.9°

Fig. 4. Visualization of boundary layers at $Re_c=2.3\times10^4$.

was glued on the airfoil surface using double-side tape with a maximum thickness of 50 $\mu m$ . The resistance of each probe was varied in the range of 8.0~20.0Ω due to manufacturing uncertainty.

Fig. 3 shows a glue-on probe and its positions on the airfoil surface. The positions are S/C=0.044, 0.067, 0.075, 0.086, 0.256, 0.317, 0.367, 0.417, 0.475, 0.506, 0.533, 0.567, 0.572, 0.617, 0.644, 0.700, 0.899, and 0.956. The sampling frequencies were 0.840 (for $Re_c=2.3\times10^4$), 1.200 (for $Re_c=3.3\times10^4$), and 1.720 kHz (for $Re_c=4.8\times10^4$), and about 2400 samples were acquired per cycle. The signal was simultaneously recorded with a trigger pulse that was generated at an angle-of-attack of 0°. The instantaneous signal on the different periods was caught for each measurement station, and special attention was given to catch the typical signal pattern. The obtained data was normalized by its mean value per cycle.

## 3. Results and discussion

### *3.1 Unsteady boundary-layers visualization*

Flow visualizations were performed according to the scheme described in the previous section in order to obtain physical insight into the unsteady boundary layers. On the other hand, the boundary layer flow experienced disturbances besides buoyancy of wire heating because the smoke-wire was installed inside the boundary layer. Furthermore, the disturbances could differ with respect to the instantaneous angle-of-attack or Reynolds number. In fact, it was difficult to estimate the wire effects in the boundary layer due to the airfoil movement. However, the Reynolds number based on the wire diameter was fortunately less than 36, which is similar to the value that has been suggested by Batill and Muller [17]. Also, the disturbances caused by the wire were stabilized due to the favourable pressure gradient faced immediately after passing the wire. Figs. 4(a), 4(b) [18] show the boundary-layers visualization at downstroke -3° (Fig. 4(a)) and upstroke 3° (Fig. 4(b)) for $Re_c=2.3\times10^4$, respectively. For a symmetric airfoil, the boundary layer flow on the upper side at upstroke 3° has similar properties to that on the lower side at downstroke -3°. Thus, Figs. 4(a), 4(b) indirectly show the wire effects in the boundary layer. As a result, if there were significant flow disturbances caused by the wire, the boundary layer breakdown or broken near-wake structure would be observed in the visualization. However, as seen in Fig. 4, they were not observed, meaning that we were able to obtain reasonable results from the visualization.

In the present paper, flow patterns of four types were observed for the visualization at $Re_c=2.3\times10^4$. First, the smoke streak comes from the vicinity of the leading edge and flows to the trailing edge along the airfoil surface without the breakdown of smoke streak (pattern Ⅰ). Normally, this pattern turns up in the downstroke of a negative angle-of-attack (Fig. 4(a)), and in this case, it is evident that the flow of boundary layer was attached and accelerated. Second, pattern Ⅱ is similar to pattern Ⅰ, but spacing between the airfoil surface and the smoke streak was observed over the trailing edge (Fig. 4(b)). The spacing grew as it went towards the trailing edge, and the position at which the spacing started moved to the leading edge with the increase of angle-of-attack. Thirdly, pattern Ⅲ was observed for a stationary airfoil (Fig. 4(c)). In this case, the laminar separation, accompanied with boundary layer breakdown, was clearly observed. Kim et al. [19] measured the boundary layers for the stationary NACA0012 airfoil in the same facility and at the same Reynolds number that was employed in the present study. In their study, the laminar separation occurred near S/C=0.26 at the angle-of-attack of 6°. This result agrees with that in Fig. 4(c). Finally, pattern Ⅳ was obtained for a pitching airfoil (Fig. 4(d)). In pattern Ⅳ, the spacing (black part near the airfoil surface around the quarter chord in Fig. 4(d)) between the airfoil surface and the

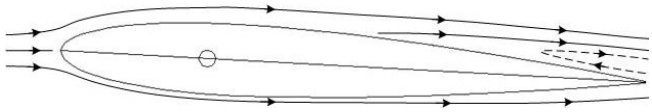

(a) Schematic of pattern Ⅱ (Fig. 4(b))

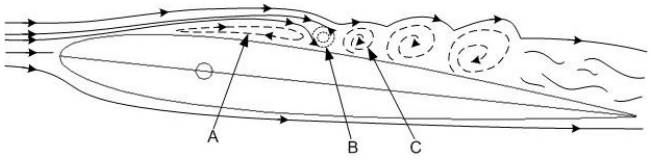


(b) Schematic of pattern Ⅳ (Fig. 4(d))

Fig. 5. Schematics of boundary layer patterns at $Re_c=2.3\times10^4$.

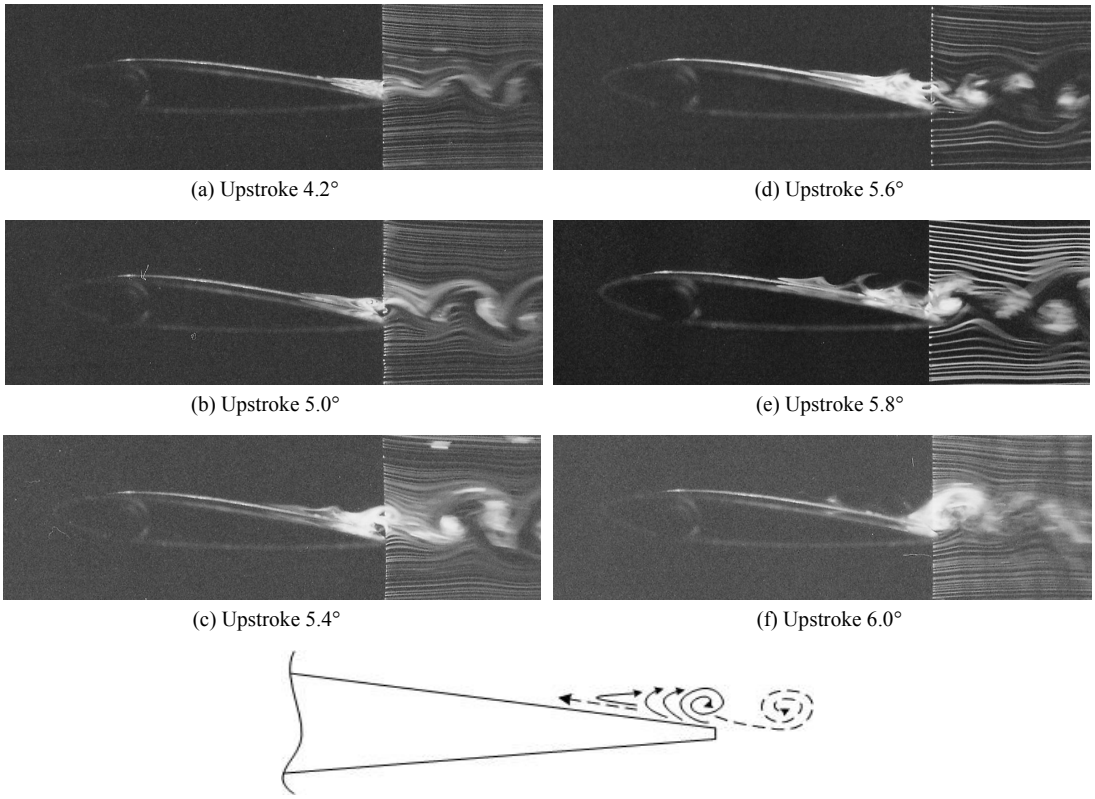

(a) Upstroke 4.2° (d) Upstroke 5.6°

(b) Upstroke 5.0° (e) Upstroke 5.8°

(c) Upstroke 5.4° (f) Upstroke 6.0°

(g) Schematic of the flow over the tailing edge

Fig. 6. Visualization of reverse flow at $Re_c=2.3\times10^4$.

smoke streak over the quarter-chord position was clearly increased with going downstream. In this case, the smoke streak was broken-down over the airfoil surface, accompanying with the formation of discrete vortices, and the discrete vortices grew along the airfoil surface, undergoing an adverse pressure gradient.

In the results obtained from the visualization, the patterns Ⅰ and Ⅲ are typical and give persuasive information about the boundary layer development. However, the patterns Ⅱ and Ⅳ are unusual and their flow schematics are described in Fig. 5. The pattern Ⅱ started from the upstroke 3° at $Re_c=2.3\times10^4$, and the point at which the spacing started was observed at a lower angle-of-attack with the increase of Reynolds number. It moved towards the leading edge with the increase of angle-of-attack. The behavior of the point is very similar to that of a laminar separation point, which was confirmed by the zero shear stress value at that point (see Fig. 11(a)), indicating the occurrence of laminar separation.

As mentioned earlier, criterions of laminar separation and unsteady laminar separation are different [5-8], which means that the unsteady laminar separation is out of accordance with the zero shear stress. In the present paper, the unsteady laminar separation is depicted in Fig. 5(b), which shows the schematic of pattern Ⅳ. In Fig. 5(b), the separated flow over the leading edge is reattached by the vortex B, which rotates in the opposite direction against the streamwise direction, accompanying with the formation of separation bubble A. Again, as the vortex C, which rotates in the streamwise direction, is gener-

ated, a saddle point is produced by the vortices B, C, the wall, and the external flow. At this point, the unsteady laminar separation can be predicted. This flow pattern of the unsteady laminar separation is similar to the results found by Koromilas and Telionis [8], who have suggested the unsteady laminar separation in a cylindrical body (see Fig. 48 in their study). In their study, the vortex B with a relatively small scale was generated by the vorticity balance between separations bubble A and vortex C. However, the vortex B appears to be independently generated with a large scale in the flow going downstream in the present paper. Actually, Fig. 5(b) shows the schematic of Fig. 8(c), which describes the pattern Ⅳ at its best. The separation bubble A, the vortices B and C were generated along the airfoil surface one after the other. This seems to be caused by both a moderate adverse pressure gradient and boundary layer thinning in the geometrical issue. As a result, the saddle point (unsteady laminar separation) was isolated from the reattachment point and yielded the unsteady laminar separation point downstream of the reattachment point. Accordingly, in a low Reynolds number range, unsteady laminar separation in moderate adverse pressure gradient seems to occur as a result of vortex interaction in the process of transition by the reattachment of the separated boundary layer. On the other hand, in the present paper, a reverse flow was not observed during the downstroke (see Fig. 6); however, the discrete vortices which indicate the unsteady laminar separation were still observed over the airfoil surface (see Figs. 8(d), 8(e), and 8(f)). This means that reverse flow is not an indicator of the unsteady laminar separation for a pitching airfoil any more, and discrete vortices are formed by the unsteady laminar separation.

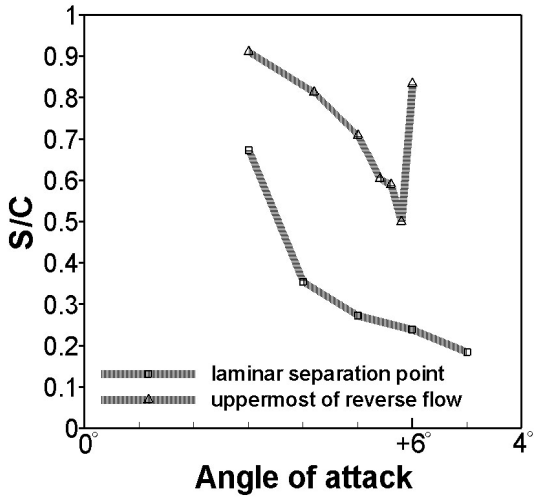


Fig. 7. Laminar separation point and uppermost of reverse flow at $Re_c=2.3\times10^4$.

To figure out the reverse flow, flow visualization was carried out using a smoke wire that was installed 3mm downstream from the trailing edge. The results for the case of $Re_c=2.3\times10^4$ are chronologically shown in Fig. 6. Actually,

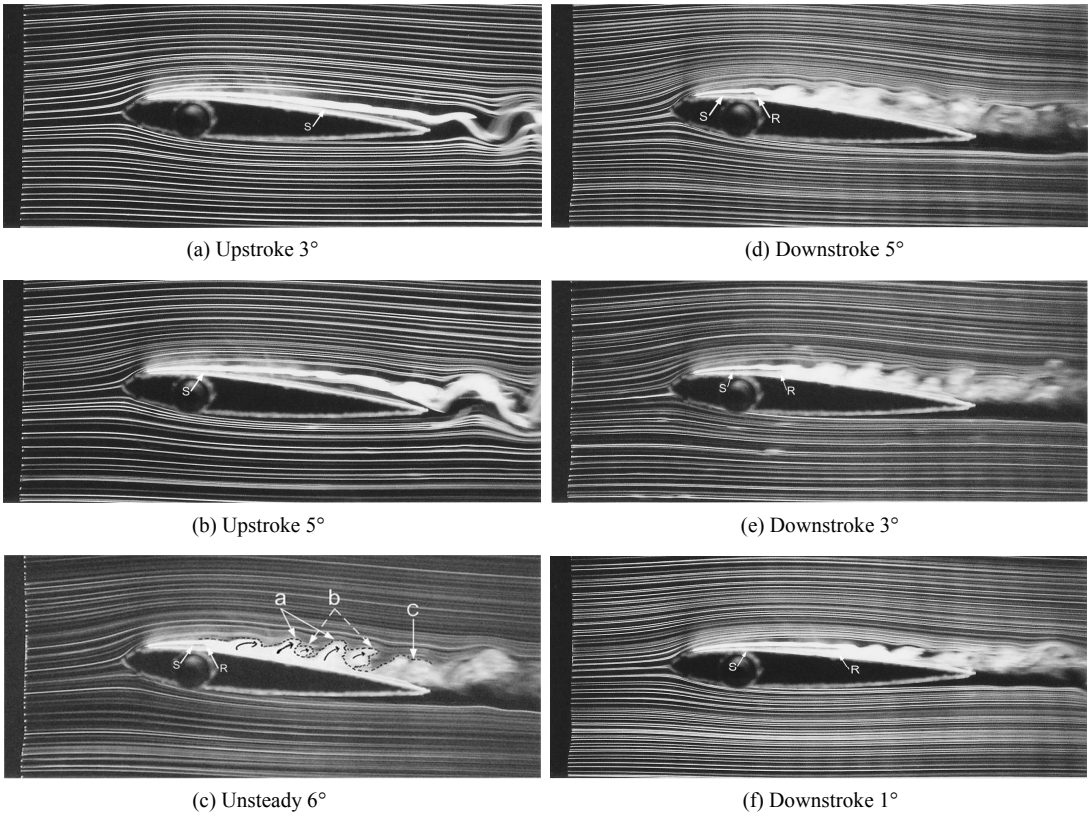


(a) Upstroke 3° (d) Downstroke 5°

(b) Upstroke 5° (e) Downstroke 3°

(c) Unsteady 6° (f) Downstroke 1°

Fig. 8. Visualization of the boundary layers at $Re_c=2.3\times10^4$.

the results seen in Fig. 6, representing the occurrence of unsteady laminar separation (Fig. 6(e)) and the trailing edge stall (Fig. 6(f)), agree well with that of Kim and Park [9]. However, in Fig. 6, a trailing edge vortex that rotated in the streamwise direction was obviously observed (Figs. 6(a), 6(b), 6(c), and 6(d)) over the trailing edge. This was not found in Kim and Park [9]. The trailing edge vortex seems to be generated by the interaction between the flow in the vicinity of the trailing edge and the airfoil motion. The trailing edge vortex begins to be broken down by the occurrence of unsteady laminar separation (Fig. 6(e)), and it was completely broken-down in the initial stage of the downstroke.

Fig. 6(g) shows the schematic of the trailing edge vortex around the trailing edge and the following flow structure in the near-wake region. The trailing edge vortex rotated in the streamwise direction, whereas the followed vortex rotated in the opposite direction against the streamwise direction. In this situation, the following vortex could induce the reduction of drag and the generation of propulsion because it is located on the upper side of wake. Such a flow pattern is a basic principle to reduce drag in the flow circumstance for a pitching airfoil [20].

On the other hand, reverse flow and boundary layer breakdown have been regarded as an indicator of separation for a stationary airfoil; however, boundary layer breakdown does not occur even though reverse flow is generated for a pitching airfoil. The reverse flow was observed from about upstroke 3° to the maximum angle-of-attack, but it was not observed in the downstroke. For a stationary airfoil, the boundary layer breakdown generally occurs when the uppermost of the reverse flow corresponds with the laminar separation point. However, for a pitching airfoil, the uppermost of the reverse flow did not reach the laminar separation point because the time scales of the laminar separation and the reverse flow are essentially different, as seen in Fig. 7. Fig. 7 shows the uppermost of the reverse flow obtained in Fig. 6 and the laminar separation point obtained during the upstroke (the case in which reattachment does not occur) in Fig. 8. Substantially, the difference of time scales between the laminar separation and the reverse flow appears to be induced by the trailing edge vortex. That is, as the trailing edge vortex disturbs the reverse flow that propagates towards the upstream, the uppermost of the reverse flow does not reach to the laminar separation point, and this essentially results from the pitching motion of the airfoil.

Figs. 8 and 9 show the chorological boundary-layers visualization for $Re_c=2.3\times10^4$ and $3.3\times10^4$ from upstroke 3° to downstroke 1° with some interval. The laminar separation and the reattachment points were roughly estimated and are marked in the figures. The unsteady laminar separation occurs at the close downstream of reattachment, and it is not marked.

In the case of $Re_c=2.3\times10^4$ (Fig. 8), the laminar separation ('S') occurred and climbed towards the leading edge during the upstroke and moved towards the trailing edge during the downstroke. Around the angle-of-attack of 6° (maximum angle-of-attack), since the motion direction of the airfoil changed abruptly, the airfoil was instantaneously lying in a quasi-steady state. Then the separated boundary layer was reattached ('R' in Fig. 8(c)), accompanied with the formation of a separation bubble of about 5% ($l_b/C$), and discrete vortices similar to Kármán vortex were generated on the airfoil surface, indicating the occurrence of unsteady laminar separation. In Fig. 8(c), discrete vortices of 'a' and 'b' were generated from the different oil droplets on the smoke-wire; thus three vortices were formed from about 0.35C to 0.75C, except the area around the trailing edge. The vortices grew towards the trailing edge and were largely separated over the trailing edge ('c' in Fig. 8(c)) due to the trailing edge stall that is shown in Fig. 6(f).

Chang [13] suggested that the velocity defect and width of near-wake are associated with the flow properties of an unsteady boundary layer. In his study, the velocity defect and width of near-wake were distinguished between $Re_c=5.3\times10^4$ and $1.9\times10^4$. Actually, this result, meaning the formation of the discrete vortices at low Reynolds number for an unsteady boundary layer, may be a reason for the results in Chang [13]. The vortices, which are laminar flow, induce a stronger vortex interaction in the near-wake region (see Figs. 8 and 9). As a result, the defect velocity becomes large, and the width widens in the near-wake for a pitching airfoil.

The flow patterns at $Re_c=3.3\times10^4$ (Fig. 9) are almost similar to those for the case of $Re_c=2.3\times10^4$ except for a few differences. Namely, the laminar separation, the reattachment, and the unsteady laminar separation occur at a lower angle-of-attack than that of $Re_c=2.3\times10^4$ in the upstroke. For $Re_c=3.3\times10^4$, the discrete vortices start to be generated at upstroke 5°, accompanied with a separation bubble of 4.9% ($l_b/C$). During the downstroke, the laminar separation, the reattachment, and the unsteady laminar separation remain upstream when compared to those of $Re_c=2.3\times10^4$. As a result, the increase of Reynolds number promotes (delays) laminar separation, reattachment, and unsteady laminar separation during upstroke (downstroke) for a pitching airfoil. These results agree well with those of Schreck et al. [21, 22], who investigated the boundary layer events for a pitching airfoil using shear stress measurement. At $Re_c=3.3\times10^4$, the discrete vortices generated from the unsteady laminar separation were broken-down early compared to those of $Re_c=2.3\times10^4$, and the boundary layer rapidly transitioned to a turbulent flow over the trailing edge due to the entrainment of external flow. The entrainment marked with arrows in Fig. 9(d) was confirmed by a short movie, and its strength is the largest about downstroke 5°. For $Re_c=4.8\times10^4$, the discrete vortices over the airfoil surface were not observed due to rapid transition, and the laminar separation, the reattachment, and the unsteady laminar separation were unfortunately not perceived (not shown). However, it is obvious that the formation of separation bubble and the discrete vortices generation by unsteady laminar separation are attributed to the low Reynolds number effects.

Actually, for a stationary airfoil in which laminar flow is predominant, a laminar separation bubble does not occur be-

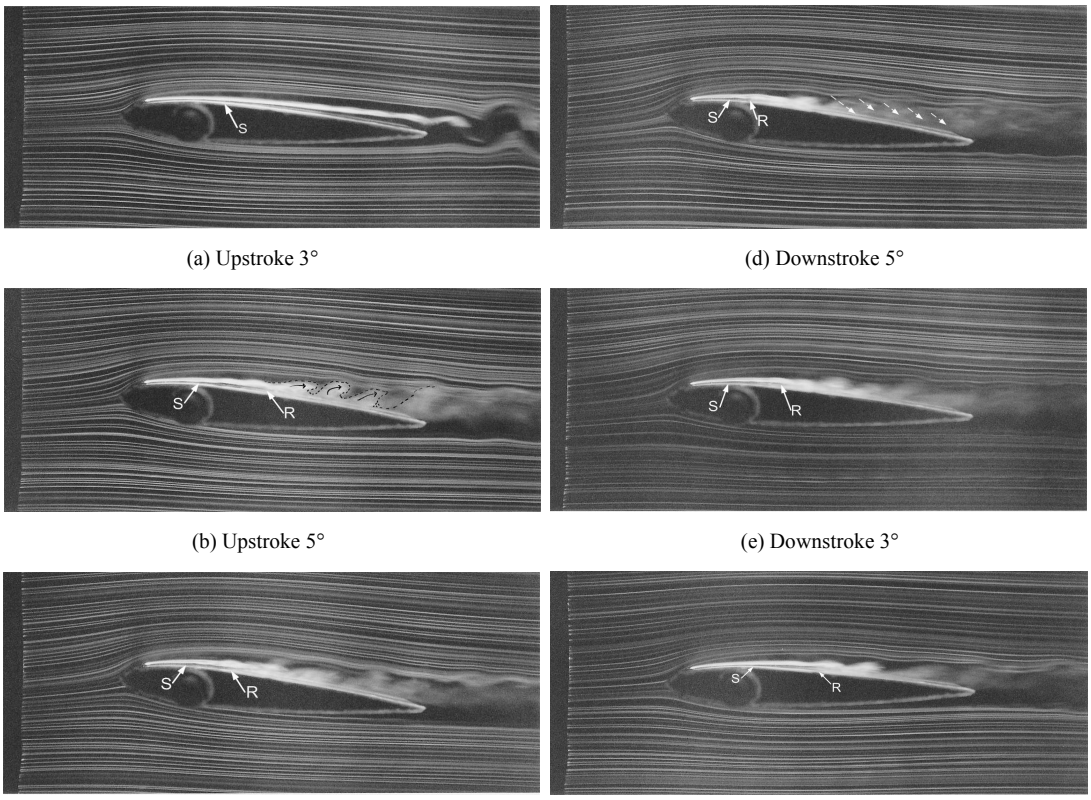


(a) Upstroke 3° (d) Downstroke 5°

(b) Upstroke 5° (e) Downstroke 3°

(c) Unsteady 6° (f) Downstroke 1°

Fig. 9. Visualization of the boundary layers at $Re_c=3.3\times10^4$.

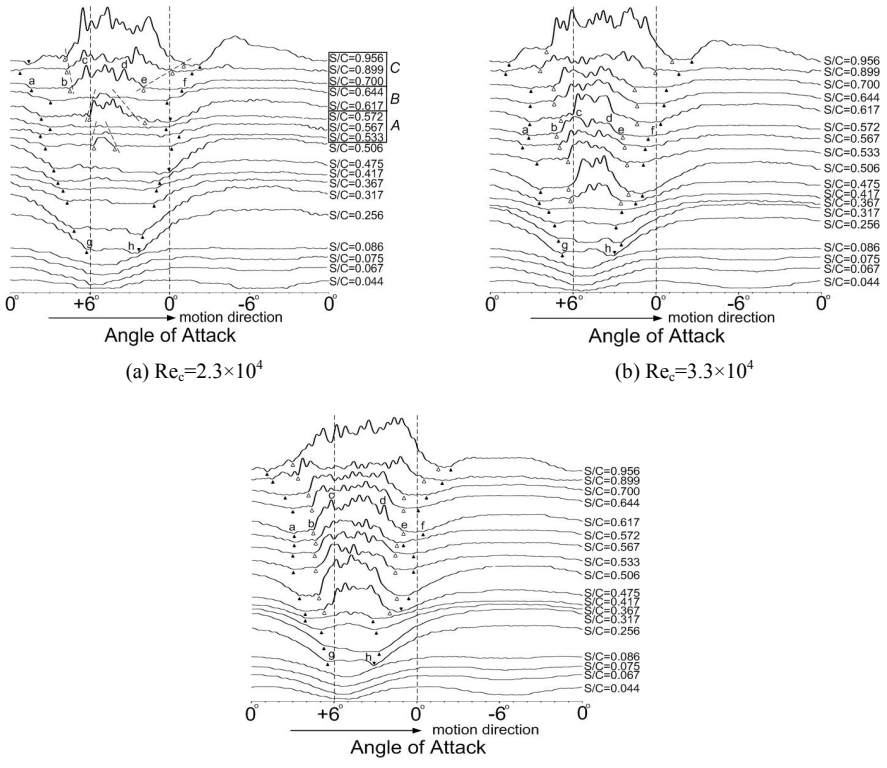


(a) $Re_c=2.3\times10^4$ (b) $Re_c=3.3\times10^4$

(c) $Re_c=4.8\times10^4$

Fig. 10. Surface-mounted probe signals according to Reynolds numbers.

low $Re_c=5.0\times10^4$. In this regime, the Reynolds number based on the bubble length is about $5.0\times10^4$ (Carmichael [23]), which means that the chord Reynolds number has to be larger than $5.0\times10^4$ in order to form the laminar separation bubble. However, in the present case, which is less than $Re_c=5.0\times10^4$, the laminar separation bubble was observed. The Reynolds number based on the bubble length was between $0.2\times10^4$~ $1.4\times10^4$ for the cases of $Re_c=2.3\times10^4$ and $3.3\times10^4$, and they are much lower than those of a stationary airfoil. This indicates that the boundary layer events, which are produced above $Re_c=5.0\times10^4$, can occur at lower Reynolds numbers by an unsteady effect. The conclusion is thus that the unsteady flow effect enhances the recovery pressure, which is necessary for reattachment, by the rotational force in the rear part of the quarter chord.

### *3.2 Surface-mounted probe signals*

Fig. 10 shows the normalized surface-mounted probe (glue-on probe) signals for the given Reynolds numbers in temporal and spatial domains. The ordinate denotes the normalized distance (S/C) from the leading edge along the airfoil surface, while the abscissa denotes the variation of angle-of-attack. The signals were normalized by each mean value per cycle, and the regions of 0°→+6° and -6°→0° represent the upstroke, while +6°→-6° represents the downstroke. As mentioned earlier, since the probes were not calibrated, the obtained data does not depict a physical meaning. The signals, hence, were analyzed with boundary-layers visualization.

In Fig. 10, the signals patterns can be separated into two regions: positive and negative angle-of- attack. Interesting variations in the signals were observed on the positive angle-of-attack since the side on which the probes were installed acted as a lifting surface. Overall patterns of the signals show a typical pattern; however, there are two interesting results in the present paper. First, in the regions of 0°→+6° and +6°→0°, the signals reach a minimum value during some time ('plateau region', 'a'-'b' and 'e'-'f'). Recently, Lee and Basu [24], Lee et al. [25], and Lee and Gerontakos [26] used multiple hot-

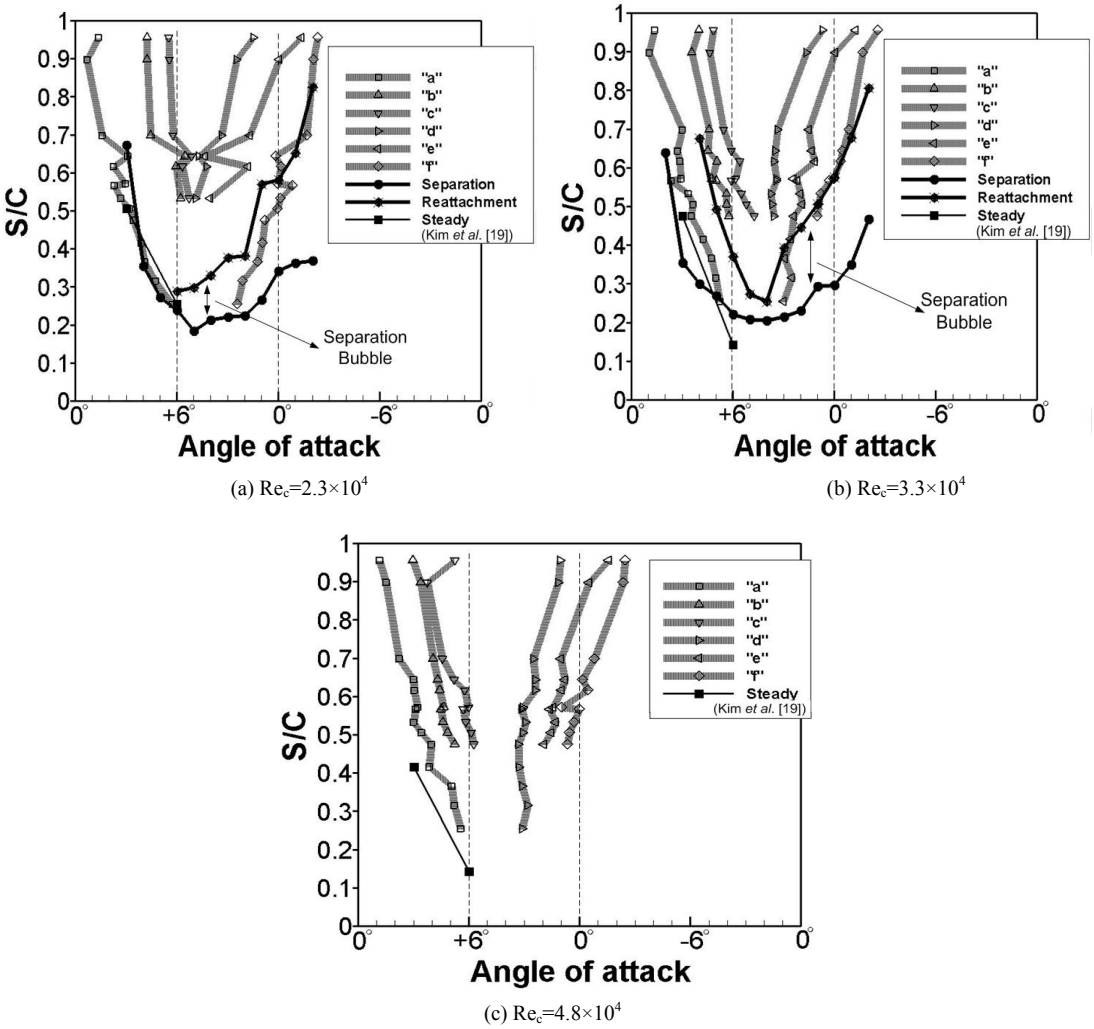


(a) $Re_c=2.3\times10^4$

(b) $Re_c=3.3\times10^4$

(c) $Re_c=4.8\times10^4$

Fig. 11. Laminar separation and reattachment point obtained from boundary-layers visualization and glue-on probes signals according to Reynolds numbers.

film sensors for the measurement of unsteady boundary layers at $Re_c=1.35\times10^5$. However, the plateau regions in the upstroke and downstroke were not found in their study. Accordingly, the plateau region, which was observed in all present cases, shows the flow features in low Reynolds number even if we consider the probe error and no calibration.

On the other hand, another interesting point in Fig. 10 is the Reynolds number effects for an unsteady boundary layer. As shown in Fig. 10, the fluctuations of the signals that present a turbulent flow largely differ between $Re_c=2.3\times10^4$ and $3.3\times10^4$ over the trailing edge. In the former case, the signal patterns over the trailing edge are classified into three regions (A, B, and C in Fig. 10(a)) in the spatial domain in the positive angle-of-attack. In that region, the duration time of fluctuations discontinuously is increased as they approach the trailing edge. If we consider the results of Fig. 8(c), we can observe that regions 'A', 'B', and 'C' coincide with the discrete vortices 'a' and 'c' of the visualization of $Re_c=2.3\times10^4$, which implies that the shear stress is locally increased by the discrete vortices. Consequently, the discrete vortices formed by the unsteady laminar separation are critically influenced by Reynolds number in the low Reynolds number range, and they formed below $Re_c=3.3\times10^4$ in the present paper.

Fig. 11 shows the critical lines of surface-mounted probe signals as well as the laminar separation and the reattachment point. The critical lines of the surface-mounted probe signals that manifest the shear stress variation were selected in Fig. 10 and are marked as 'a', 'b', 'c', 'd', 'e', and 'f' in Fig. 11. Also, the laminar separation and the reattachment obtained from the unsteady boundary-layers visualization (Figs. 8 and 9) are presented along the surface coordinate. The 'steady' shows the laminar separation for a stationary airfoil, and it was obtained from Kim et al. [19].

In Fig. 11, at $Re_c=2.3\times10^4$, during the upstroke, the laminar separation and the zero shear stress obtained for a pitching airfoil correspond well to the laminar separation obtained for a stationary airfoil. As Reynolds number increases, the laminar separation for a pitching airfoil becomes a non-linear pattern, and the zero shear stress variation is delayed when compared to the laminar separation obtained for a stationary airfoil during upstroke.

Note that in the low Reynolds number range, the laminar separation, reattachment, and unsteady laminar separation simultaneously occurred over the airfoil surface for a pitching airfoil. In the upstroke, the laminar separation appears to be well matched to the zero shear stress point (inception of plateau; line 'a') at $Re_c=2.3\times10^4$ for a pitching airfoil. This suggests that the rough estimate of the laminar separation point from the unsteady boundary-layers visualization is reasonable. As Reynolds number increases, the reattachment and unsteady laminar separation occur during the upstroke ($Re_c=3.3\times10^4$), and then the laminar separation is promoted against zero shear stress. Also, at $Re_c=3.3\times10^4$, the reattachment point and the unsteady laminar separation point seem to correspond to the point at which the shear stress starts to increase (end of plateau; line 'b'), implying the boundary layer transition. This means that the inception and the end of the plateau region correspond with the laminar separation and the reattachment (unsteady laminar separation), respectively. The boundary layer transition occurs from the breakdown of discrete vortices generated after the unsteady laminar separation, and it can be reconfirmed by the fluctuation of the surface-mounted probe signals, which manifests a turbulent flow.

During the downstroke, the inception and the end of the plateau region do not correspond with the laminar separation or the reattachment point. Actually, in the author's opinion, the reattachment point obtained from the unsteady boundary-layers visualization may have to correspond to the line 'e', which indicates the inception of the plateau, and the laminar separation point may have to follow line 'f', which indicates the end of the plateau during the downstroke (see Figs. 11(a) and 11(b)). However, the laminar separation and the reattachment point occur upstream when compared to lines 'e' and 'f', respectively. During the downstroke, laminar separation, reattachment, and zero shear stress points move towards the trailing edge, and thus the conclusion is that the laminar separation and the reattachment point are significantly delayed compared to the zero shear stress during the downstroke.

## 4. Conclusions

Smoke-wire visualization and qualitative shear stress measurements were carried out in order to investigate unsteady boundary layers in a low Reynolds number range. The tests were intensively conducted for Reynolds numbers $2.0\times10^4$~$5.0\times10^4$.

For a pitching NACA0012 airfoil, the separation bubble was formed by reattachment within the stall angle, and unsteady laminar separation was observed at the saddle point by two vortices, wall, and external flow. Then the laminar separation, the reattachment, and the unsteady laminar separation simultaneously occurred over the airfoil. The unsteady laminar separation occurred downstream of the reattachment and was independent on reverse flow. Thus, unsteady laminar separation occurs in the process of transition after the reattachment of the separated boundary layer. The discrete vortices are formed by the unsteady laminar separation, and its formation is ultimately affected by Reynolds number. The reverse flow observed over the trailing edge significantly interacted with the trailing edge vortex that rotates in the streamwise direction. This trailing edge vortex prevents the uppermost of the reverse flow from reaching the unsteady laminar separation point during the upstroke; this induces that the boundary layer breakdown does not occur in spite of the occurrence of laminar separation. The boundary-layer breakdown, reverse flow, and zero shear stress do not coincide for a pitching airfoil. The reattachment and the unsteady laminar separation are promoted (delayed) by the increase of Reynolds number during the upstroke (downstroke). The laminar separation is promoted (delayed) against the zero shear stress dur-

ing the upstroke (downstroke) with Reynolds number.

## Acknowledgments

This work was supported by the Korea Research Foundation Grant funded by the Korea Government (MOEHRD, Basic Research Promotion Fund) (KRF-2007-313-D00124).

## Nomenclature

| | | |
|---|---|---|
| C | : | Chord length |
| $K$ | : | Reduced frequency |
| $l_b$ | : | Separation bubble length |
| $S$ | : | Distance from the leading edge along the airfoil surface |
| $t$ | : | Time |
| $U_\infty$ | : | Free-stream velocity |
| $\alpha$ | : | Angle-of-attack |
| $\rho$ | : | Air density |
| $\omega$ | : | Angular velocity of an oscillating airfoil |
| $Re_c$ | : | Reynolds number based on chord length |

## References

[1] W. J. McCroskey, Unsteady Airfoils, *Ann. Rev. Fluid Mech*. 14 (1982) 285-311.

[2] M. Pascazio, J. M. Autric, D. Favier and C. Maresca, Unsteady boundary-layer measurement on oscillating airfoils: Transition and separation phenomena in pitching motion, AIAA paper 96-0035.

[3] L. E. Ericsson and J. P. Reding, Fluid mechanics of dynamics stall Part 1. Unsteady flow concepts, *J. Fluids and Structure* 2 (1988) 1-33.

[4] L. E. Ericsson, Moving wall effect in relation to other dynamic stall flow mechanics, *J. Aircraft* 31 (1994) 1303-1309.

[5] W. R. Sear and D. P. Telionis, Boundary-layer separation in unsteady flow, SIAM *J. Appl. Math*. 28 (1975) 215-235.

[6] D. T. Tsahalis and D. P. Telionis, Oscillating laminar boundary layers and unsteady separation, *AIAA J.* 12 (1974) 1469-1475.

[7] R. A. Despard and J. A. Miller, Separation in oscillating laminar boundary-layers flows, *J. Fluid Mech*. 47 (1971) 21-31.

[8] C. A. Koromilas and D. P. Telionis, Unsteady laminar separation: an experimental study, *J. Fluid Mech*. 97 (1980) 347-384.

[9] J. S. Kim and S. O. Park, Smoke wire visualization of unsteady separation over an oscillating airfoil, *AIAA J*. 26 (1988) 1408-1410.

[10] S. O. Park, J, S. Kim and B. I. Lee, Hot-Wire Measurement of near-wakes behind an oscillating airfoil, *AIAA J*. 28 (1989) 22-28.

[11] K. Ohmi, M. Coutanceau, T. P. Loc and A. Dulieu, Vortex formation around an oscillating and translating airfoil at large incidence, *J. Fluid Mech*. 211 (1990) 37-60.

[12] H. Oshima and B. R. Ramaprian, Velocity measurements over a pitching airfoil, *AIAA J*. 35 (1997) 119-126.

[13] J. W. Chang, Near-wake characteristics of an oscillating NACA 4412 airfoil, *J. Aircraft* 41 (2004) 1240-1244.

[14] E. V. Laitone, Aerodynamic lift at reynolds numbers below $7\times10^4$, *AIAA J*. 34 (1996) 1941-1942.

[15] E. V. Laitone, Wind tunnel tests of wings at Reynolds numbers below 70000, *Exps. Fluids* 23 (1997) 405-409.

[16] H. H. Bruun, *Hot-Wire Anemometry* Oxford University Press, (1995) 272-286.

[17] S. M. Batill and T. J. Mueller, Visualization of Transition in the flow over an airfoil using the smoke-wire technique, *AIAA J*. 19 (1981) 340-345.

[18] D. H. Kim and J. W. Chang, Reynolds number effects on unsteady boundary layer of an oscillating airfoil, AIAA Paper 2009-3501.

[19] D. H. Kim, J. H. Yang, J. W. Chang and J. Chung, Boundary layer and near-wake measurements of NACA 0012 airfoil at low reynolds numbers, AIAA Paper 2009-1472.

[20] M. M. Koochesfahani, Vortical patterns in the wake of an oscillating airfoil, *AIAA J*. 27 (1989) 1200-1205.

[21] S. J. Schreck, W. E. Faller and H. E. Helin, Pitch rate and Reynolds number Effects on Unsteady Boundary Layer Transition and Separation, *J. Aircraft* 35 (1998) 46-52.

[22] S. J. Schreck, W. E. Faller and M. C. Robinson, Unsteady separation processes and leading edge vortex precursors: pitch rate and reynolds number influences, *J. Aircraft* 39 (2002) 868-875.

[23] B. H. Carmichael, Low reynolds number airfoil survey-Volume 1, NACA Contractor Report 165803 (1981).

[24] T. Lee and S. Basu, Measurement of unsteady boundary layer developed on an oscillating airfoil using multiple hot-film sensors, *Exps. Fluids* 25 (1998) 108-117.

[25] T. Lee, G. Petrakis, F. Mokhtarian and F. Kafyeke, Boundary-layer transition, separation, and reattachment on an oscillating airfoil, *J. Aircraft* 37 (1999) 356-360.

[26] T. Lee and P. Gerontakos, Investigation of flow over an oscillating airfoil, *J. Fluid Mech.* 512 (2004) 313-341.

**Dong-Ha Kim** received his B.S. degree from the Department of Aerospace and Mechanical Engineering in 2003, and received his M.S. in 2005 from Korea Aerospace University. He is currently a Ph.D. candidate in Korea Aerospace University. His research interests include unsteady aerodynamics and wind tunnel experiments.

**Jo-Won Chang** received his B.S. in Aerospace Engineering from the Korean Air Force Academy in 1982, and his M.S. and Ph.D. degrees from Seoul National University and KAIST in 1986 and 1999, respectively. He is currently an associate professor in the Department of Aeronautical Science and Flight Operation at Korea Aerospace University in Korea. His research interests include unsteady aerodynamics, bio-fluid mechanics, wind tunnel experiments, and flight tests.